Neuper & Klimesch (Eds.)
Progress in Brain Research, Vol. 159
ISSN 0079-6123

CHAPTER 9

Analyzing event-related EEG data with multivariate autoregressive parameters

Alois Schlögl[1,*] and Gernot Supp[2,3]

[1]*Institute for Human–Computer Interfaces, University of Technology at Graz, Graz, Austria*
[2]*Department of Neurophysiology and Pathophysiology, Center of Experimental Medicine, University Medical Center Hamburg-Eppendorf, University of Hamburg, Hamburg, Germany*
[3]*Max Planck Institute for Human Cognitive and Brain Sciences, Leipzig, Germany*

Abstract: Methods of spatio-temporal analysis provide important tools for characterizing several dynamic aspects of brain oscillations that are reflected in the human scalp-detected electroencephalogram (EEG). The search to identify the dynamic connectivity of brain signals within different frequency bands, in order to uncover the transient cooperation between different brain sites, converges at the potential of multivariate autoregressive (MVAR) models and their derived parameters. In fact, MVAR parameters provide a whole battery of so-called coupling measures including classic coherence (COH), partial coherence (pCOH), imaginary part of coherence (iCOH), partial-directed coherence (PDC), directed transfer function (DTF), and full frequency directed transfer function (ffDTF). All of these approaches have been developed to quantify the degree of coupling between different EEG recording positions, with the specific aim to characterize the functional interaction between neural populations within the cortex. This work addresses the application of MVAR models to event-related brain processes, including different statistical approaches, and reviews most relevant findings in the expanding field of coupling analysis. Finally, we present several examples of coupling patterns associated with certain types of movement imagery.

Keywords: EEG coupling; brain connectivity; event-related oscillations; spatio-temporal analysis; parametric modeling

Introduction

Oscillations were one of the first phenomena observed in human electroencephalogram (EEG). The dynamics of these oscillations, like the synchronization and desynchronization of the alpha rhythm during closed and open eyes, has been already described and investigated by Hans Berger in the 1930s. With the advent of digital computers, digital signal processing methods were applied to EEG in the late 1960s. Autoregressive parameter estimation of EEG was among the first methods to uncover the signals' spectral characteristics (Lustick et al., 1968; Fenwick et al., 1969, 1970a, b, 1971; Zetterberg, 1969; Gersch, 1970; Pfurtscheller and Haring, 1972). In order to investigate the dynamics of EEG oscillations, a method to quantify event-related desynchronization (ERD) and synchronization (ERS) patterns was developed (Pfurtscheller and Aranibar, 1977; Pfurtscheller and Lopes da Silva, 1999). Essentially, this approach provides an *univariate* analysis that uncovers the spectral properties of a single EEG channel (temporal correlation within the investigated time series). Even if univariate methods are applied to

*Corresponding author. E-mail: alois.schloegl@tugraz.at

DOI: 10.1016/S0079-6123(06)59009-0

each EEG channel, no information regarding the correlation between two (or more) channels is obtained. Therefore, any ongoing coupling between EEG positions that may originate from the oscillatory interactions between spatially distant cortical populations remains undetected. Recent research, however, revealed the crucial importance of cortical couplings to brain functions, often addressed as "long-range synchronization" of oscillatory activities between distant neuronal populations. Importantly, this process should be reflected in the degree of coupling between electrode pairs (Varela et al., 2001; Gruber et al., 2002; Fiebach et al., 2005; Fries, 2005).

Certainly, coherence is the most traditional approach proposed to detect cooperative neuronal activity in electrophysiological signals. Coherence can be considered as the correlation in the frequency domain between two channels (Gardner, 1992; Varela et al., 2001). High values of coherence between two EEG signals are often interpreted as evidence for ongoing cooperation and long-range synchronization. Unfortunately, this interpretation of coherence values is distorted by two confounding factors, namely, volume conduction and the influence of common reference electrodes (Nunez et al., 1997, 1999; Florian et al., 1998; Andrew and Pfurtscheller, 1999; Pfurtscheller and Andrew, 1999). Both factors can cause the recording of the same signal simultaneously at many electrodes, which causes large coherence values even in the absence of any cortical interaction. In the recent years, several approaches were proposed on the basis of MVAR modeling (e.g., directed transfer function (DTF), partial-directed coherence (PDC), and imaginary coherence (iCOH)) to overcome these difficulties (Kaminski and Blinowska, 1991; Kaminski et al., 1995, 1997, 2001; Sameshima and Baccala, 1999; Baccala and Sameshima, 2001; Blinowska et al., 2004;Kus et al., 2004; Nolte et al., 2004). In this study, we present these MVAR-based coupling measures in detail. To demonstrate the remarkable potential of the different measures (power spectrum, phase, ordinary coherence, iCOH, PDC, and DTF), we present an event-related time-frequency (T–F) analysis of the entire set of measures of an EEG data set from a subject performing imagery hand movements.

The MVAR model and its estimators

An multivariate autoregressive (MVAR) model of order p is described by the following equation

$$\vec{Y}_t = A_1 \times \vec{Y}_{t-1} + A_2 \times \vec{Y}_{t-2} + \cdots + A_p \times \vec{Y}_{t-p} + \vec{X}_t,$$

whereas $\vec{Y}_t$ is the observed EEG data at time t, $\vec{X}_t$ is the innovation process, and A_k are the k-th autoregressive parameters. The innovation process $\vec{X}_t$ is a multivariate white noise process with mean $\vec{m}_X$ and covariance matrix Σ_X. The mean $\vec{\mu}_Y$ of the MVAR process is $\vec{\mu}_Y = \vec{m}_X(I_{M\times M} - \sum_{k-1}^{p} A_k)$ with the identity matrix $I_{M\times M}$ of size $M \times M$. If $\vec{X}_t$ has zero mean $\vec{m}_X = \vec{0}$, $\vec{\mu}_Y = \vec{0}$ and vice versa. If M channels are observed, $\vec{Y}_t$ and $\vec{X}_t$ are vectors of length M and $A_k = |a_{i,j}(k)|$ are matrices of size $M \times M$ with elements $a_{i,j}(k)$. The meaning of the coefficient $a_{i,j}(k)$ is the weighting factor that characterizes the contribution of channel j with lag k to channel i according to $y_i(t) = X_i(t) + \sum_{j=1}^{M}\sum_{k=1}^{p} a_{i,j}(k)y_j(t-k)$ with $i = 1,\ldots,M$. In the case $k>0$, only time-delayed contributions are modeled, and therefore, one might understand this approach as modeling causal relationships. Moreover and equally important, the coefficients $a_{i,j}(k)$ describe the direction of the connection (from channel j to i), which certainly can differ from the reversed case $a_{j,i}(k)$. Accordingly, the MVAR model is capable of describing directed causal relationships between channels. If the covariance matrix $\sum_X = |\sigma_{i,j}^2|$ of the innovation process is a diagonal matrix, then X_i and X_j are uncorrelated, and expressed as $\Sigma_{i,j} = \langle X_i \cdot X_j \rangle = 0$ for $i \neq j$. However, if X_i and X_j are correlated, an instantaneous (simultaneous) contribution to several channels exists. Baccala and Sameshima (2001) distinguished the former and the latter case as "Granger causality" and "instantaneous Granger causality," respectively.

As the very first step toward characterizing a given time series $\vec{Y}_t$, the MVAR parameters $a_{i,j}(k)$ need to be estimated. Several estimation algorithms have been proposed (Wiggins and Robinson, 1965; Marple, 1987; Schlögl, 2006). Wiggins and Robinson (1965) were the first to propose a multivariate extension of the recursive Levinson estimator for univariate AR parameters.

Therefore, this algorithm is also known as the Levinson–Wiggens–Robinson (LWR) estimator or multichannel Levinson–Durbin recursion. The univariate Burg algorithm has been extended for multivariate AR models by Nuttall and Strand (Marple, 1987; Schlögl, 2006). More recently, the least-squares estimator ARFIT has been proposed by Schneider and Neumaier (2001). A detailed comparison of various MVAR estimators (Schlögl, 2006) revealed that the multivariate Burg algorithm provides the most accurate estimates. Software implementations of the estimators mentioned above are available from the TSA toolbox for Octave and Matlab, which is included in BioSig (see http://biosig.sf.net). These implemented MVAR estimators have a very useful feature, namely they can handle data with missing values. Missing values can arise from artifact detection and occur quite often in EEG recordings. Missing values can be encoded efficiently as not-a-number (NaN) according to the IEEE 754 standard regarding the encoding of floating point numbers. The estimation algorithms are implemented so that any NaNs (i.e., missing values) are ignored. This feature is highly useful for artifact processing as well as for combining time and ensemble averages of the MVAR estimates.

Derived measures

In the following, the relation between MVAR parameters and their derived measures will be explained briefly. Our discussion includes (auto and cross) spectra, phase relations, coherency (absolute coherence and iCOH), partial coherence (pCOH), PDC, directed transfer function (DTF), and full-frequency DTF (ffDTF).

If we transform the MVAR model from the time-domain into the z-domain and the f-domain, the following transfer functions

$$H(z) = Y(z)/X(z) = \left[I - \sum_{k=1}^{p} (z^{-k} \cdot A_k) \right]^{-1} \text{ and}$$

$$H(f) = A^{-1}(f) = Y(f)/X(f)$$

are obtained, where $H(f) = H(z; z = \mathrm{e}^{2\pi i f/f_0})$ with $z = \mathrm{e}^{2\pi i f/f_0}$ (given a sampling rate f_0). From these equations, we can derive several multivariate parameters in the frequency domain:

(a) The multivariate spectral density of $\vec{Y}_t$ is $Y(f) = H(f) \cdot X(f)$ with frequency f and $\mathrm{Y}(f) = |\mathrm{Y}_{ij}(f)|$, a matrix with elements $Y_{ij}(f)$. The matrix elements $Y_{ij}(f)$. represent the cross-spectrum between channels i and j (if $i \neq j$) and the autospectra (in case $i = j$). The power spectral density of $\vec{Y}_t$ is given by $\mathrm{S}_\mathrm{Y}(f) = |Y(f)|^2$and is obtained by $S_Y(f) = H(f)\Sigma_X H^{\mathrm{H}}(f)$. The superscript indicates the *Hermitian* operator (transposed complex conjugate of matrix H).

(b) The coherency (Nolte et al., 2004) is defined as

$$C_{ij}(f) = \frac{Y_{ij}(f)}{\sqrt{Y_{ii}(f) \cdot Y_{jj}(f)}}$$

and its complex parts can be expressed as

$$C_{ij}(f) = \mathrm{Real}(C_{ij}(f)) + \sqrt{-1} \cdot \mathrm{Imag}(C_{ij}(f)) = |C_{ij}(f)| \cdot \mathrm{e}^{2\pi\sqrt{-1}\varphi_{ij}(f)}$$

The ordinary coherence is defined as the absolute value $\mathrm{COH}_{ij}(f) \equiv |C_{ij}(f)|$and in some cases the squared coherence $\mathrm{COH}_{ij}^2(f) = C_{ij}(f) \cdot C_{ij}^H(f)$ is used. Interpreting coherence as cortical coupling can be misleading, because volume conduction and activity at the reference electrodes can result in erroneous high coherence values (Florian et al., 1998; Andrew and Pfurtscheller, 1999; Pfurtscheller and Andrew, 1999).

(c) The phase difference between two channels i and j can be obtained from the cross-spectrum or the coherency according to the following equation:

$$\varphi_{ij}(f) = \mathrm{angle}(Y_{ij}(f)) = \mathrm{angle}(C_{ij}(f)) = \arctan(\mathrm{Imag}(Y_{it}(f))/\mathrm{Real}(Y_{it}(f)))$$

A phase delay between two signals different from zero indicates a time delay. Given that pure volume conduction effects appear at electrodes with a zero phase delay, phase information can be

exploited to identify true cortical propagation. The delay time of the propagation at a specific frequency f is as follows:

$$\Delta t_{ij}(f) = \varphi_{ij}(f)/(2\pi f).$$

Based on the above equation, volume conduction effects can bias the phase delay (as well as the delay in time) toward zero.

(d) Recently, Nolte et al. (2004) suggested a solution to the problem of separating volume conduction from cortical interaction. They argued that the $\mathrm{iCOH}_{ij}(f)$, defined as,

$$\mathrm{iCOH}_{ij}(f) = \mathrm{Imag}(C_{ij}(f)) = \frac{\mathrm{Imag}(Y_{ij}(f))}{\sqrt{Y_{ii}(f)\cdot Y_{jj}(f)}},$$

is exclusively caused by the occurrence of some time delay. In fact, volume conduction propagates without any time delay contributing only to the real part of coherency. Therefore, the iCOH should represent solely true cortical interactions, and is thought to be independent of any volume conduction influences.

(e) Another approach to remove volume conduction effects is to partialize the coherence. Effectively, the pCOH between channels i and j is the coherence between channel i and j, removing the (partial) components common to any other channel combination (Korzeniewska et al., 2003; Kus et al., 2004). The $\mathrm{pCOH}_{ij}(f)$ is defined as

$$\mathrm{pCOH}_{ij}(f) = \frac{g_{ij}(f)}{\sqrt{g_{ii}(f)\cdot g_{jj}(f)}},$$

whereas $g(f) = |g_{ij}(f)| = A(f)\Sigma_X^{-1}A(f)$. The pCOH is symmetric, i.e., $\mathrm{pCOH}_{ij}(f) = \mathrm{pCOH}_{ji}(f)$, therefore no directional information is obtained.

(f) In order to obtain directional information, the concept of pCOH has been extended by Baccala and Sameshima (2001), who developed the PDC measure defined as

$$\mathrm{PDC}_{ij}(f) = \frac{A_{ij}(f)}{\sqrt{\sum_{i=1}^{M}|A_{ij}(f)|^2}} = \frac{A_{ij}(f)}{\sqrt{A_{:j}^{\mathrm{H}}(f)A_{:j}(f)}}$$

with $\mathrm{A}_{:j}(\mathrm{f})$ being the j-th column of $A(f)$. The PDC measure was also used to investigate cortical couplings in the works of Supp et al. (2004, 2005). The PDC factor, $\mathrm{PDCF}_{ij}(f)$, is given by

$$\mathrm{PDCF}_{ij}(f) = \frac{A_{ij}(f)}{\sqrt{A_{:j}^{\mathrm{H}}(f)\Sigma_X^{-1}A_{:j}(f)}}.$$

Both, PDC and PDCF are related to the concept of "causality," as defined by Granger (1969). The difference between PDC and PDCF is "[the PDC] portrays exclusively Granger causality", while "[PDCF reflects a mixture with the] instantaneous Granger causality" (Baccala and Sameshima, 2001, p. 466).

(g) Another measure to uncover directed information flow is the DTF as defined by Kaminski and Blinowska (1991) (see also Kaminski et al., 1997, 2001; Blinowska et al., 2004):

$$\mathrm{DTF}_{ij}(f) = \frac{|H_{ij}(f)|}{\sqrt{\sum_{k=1}^{m}|H_{ik}^2(f)|}} = \frac{|H_{ij}(f)|}{\sqrt{H_{i:}(f)H_{i:}^{\mathrm{H}}(f)}}.$$

Later, Korzeniewska et al. (2003) and Kus et al. (2004) developed the "full frequency directed transfer function" (ffDTF)

$$\mathrm{ffDTF}_{ij}(f) = \frac{|H_{ij}(f)|}{\sqrt{\sum_f\sum_{k=1}^{m}|H_{ik}^2(f)|}} = \frac{|H_{ij}(f)|}{\sqrt{\sum_f H_{i:}(f)H_{i:}^{H}(f)}},$$

which "assures that the denominator does not change with frequency" and "shows peaks mostly for frequencies ... when there is a net flow" (Korzeniewska et al., 2003, p. 197). In order to characterize only direct connections, Korzeniewska et al. (2003) proposed to multiply the ffDTF with the pCOHs and named this new measure as dDTF:

$$\mathrm{dDTF}_{ij}(f) = \mathrm{pCOH}_{ij}(f) \cdot \mathrm{ffDTF}_{ij}(f).$$

By means of several simulations, Baccala and Sameshima (2001) could demonstrate that DTF extracts direct as well as indirect connections, whereas PDC reveals exclusively direct connections. However, Kus et al. (2004, p. 1502) described the difference between PDC and DTF as follows: "…PDC, unlike DTF, … is a ratio between the *outflow* from channel *j* to … *i* in respect to all the outflows from channel *j* (not in respect to the *inflows* to the designated channel … in case of DTF)". Hence, it is an open question, which of the two, DTF or PDC, is more advantageous in describing directional information.

Statistical significance tests

In order to evaluate whether some differences are significant or not, statistical tests need to be applied. Statistical significance tests estimate (explicitly or implicitly) some confidence interval around some estimated mean value. The confidence interval has been derived analytically for spectra and coherence (Nunez et al., 1997) as well as for iCOH (Nolte et al., 2004). Surrogate data methods have been applied by Kaminski et al. (2001) or Babiloni et al. (2005). Resampling methods such as "bootstrapping" and "jackknife" represent another interesting approach, since the underlying probability distribution does not need to be known a priori (Efron, 1981).

In this work, we apply a jackknife method, using a trial-based leave-one-out method (LOOM). All but one trial are concatenated, from which the MVAR estimates and their derived measures (COH, PDC, DTF, etc) are estimated. Then, the next trial is excluded and the parameters are estimated again. This procedure is repeated until each of the m trials has been left out once. Although the LOOM procedure is computationally expensive, it provides two advantages: (i) LOOM obtains the least-biased estimates over all other resampling methods, and (ii) no a priori assumption regarding the type of distribution is needed.

According to the LOOM approach, a sampling distribution $u = N(\mu_u, \sigma_u^2)$ is obtained. The sample distribution can be used to estimate the mean μ_u (which corresponds to the expectation value) and a standard deviation σ_u. However, the standard deviation was not obtained from m independent trials, only the (m–1)-th part of each ensemble estimate (one out of m– 1 trials) was independent. Thus, the *true* standard error for the estimate $\hat{u}$ is $\sigma_u \cdot \sqrt{m-1}$ (the validity of this approach can be demonstrated in a simple simulation using m random numbers).

In theory, also the single trial estimates could be used to obtain the mean and the standard error. However, because of the limited number of samples within one trial the model order would have to be very small, otherwise the estimation of a MVAR model would be impossible. Using ensemble averaged MVAR estimates allows larger model orders, while still using the advantages of LOOM for estimating the standard error.

The mean and the standard error are sufficient for several statistical tests (including the simple *t*-test, the paired *t*-test, and the two-sample *t*-test). In the context of this study, a simple *t*-test can be used for testing whether a certain coupling measure (such as COH, PDC, DTF, iCOH, and phase) is significantly different from zero or not. A paired *t*-test is useful for analyzing event-related changes (reference vs. activation interval) of a certain measure. For example, the paired *t*-test applied on the autospectra will provide the classical ERD and ERS analysis (Pfurtscheller and Lopes da Silva, 1999). The two-sample *t*-test can be used for testing on significant differences of different conditions (e.g., left-hand movement vs. right-hand movement, etc). In this study, we are using a two-sample *t*-test for the event-related analysis

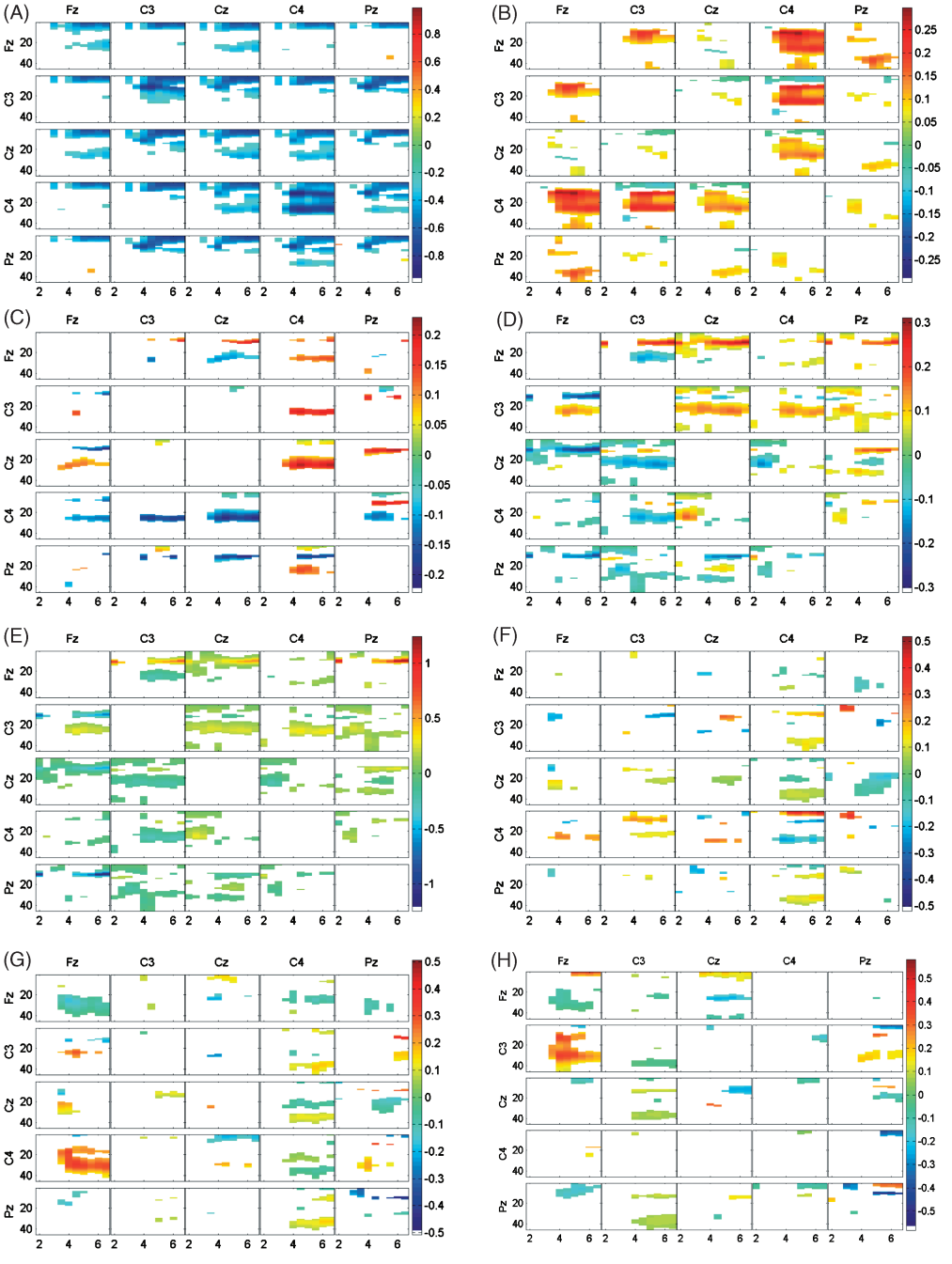
(A)
(B)
(C)
(D)
(E)
(F)
(G)
(H)
Fz
C3
Cz
C4
Pz
20
40
2
4
6

(see Figs. 1: A, B, C, F, G and H) and the simple *t*-test (Figs. D and E) for testing whether a certain measure is zero or not.

Example: EEG data of motor imagery

Now we exemplify the use of MVAR-based T–F analysis by presenting several measures derived from a single experimental data set. The subject performed a cued motor imagery task, while EEG was recorded from 60 channels (reference: left mastoid, ground: right mastoid, sampling rate: 250 Hz). The EEG was bandpass filtered between 1 and 50 Hz (Notchfilter switched on). During the experiment, the subject was seated in front of a computer screen and was guided by arrows appearing on the screen to perform one of four possible imaginary movements: left hand, right hand, foot, or tongue. The cues and therefore the type of the requested imaginary movements were randomized across the whole experiment that consisted of several runs with 40 trials each. Each trial started with a blank screen for 2 s. At second 2 a short beep-tone occurred and a fixation cross appeared on the screen to indicate the upcoming appearance of the arrow. The arrow pointing left, right, up, or down was presented at second 3 for a whole second. The subject was cued by the direction of the arrow that indicated which type of movement was requested to imagine. The subject was instructed to perform the respective motor imagery until the fixation cross disappeared (at $t = 7$ s). The data set is available online at http://ida.first.fraunhofer.de/projects/bci/competition_iii/#datasets (data set IIIa, subject k3). Some results using univariate analysis methods have been described by Schlögl et al. (2005) and Pfurtscheller et al. (2006). For the following we concentrate our investigation mostly on the data recorded during left-hand motor imagery. Five EEG positions (Fz, C3, Cz, C4, and Pz) were selected, and the MVAR parameters and their derived measures for 1-s segments (and 50% overlap) were estimated. The event-related analysis used the interval from $t = 2$ to 3 s as reference. The T–F maps are displayed for $t = 1.5$ to 7.0 s, and $f = 0$ to 45 Hz. Given that five channels are

Fig. 1. Time-Frequency maps of various coupling measures from 5 EEG channels. All coupling measures were estimated by means of a MVAR(15) model (model order 15) applied on each one-second segment (for a detailed description see text), using an overlap of 0.5 second for illustation purpose. The frequency range 0 to 45 Hz is displayed. In general, a t-ttest with $\alpha = 0.01$ was used for testing the statistical signifcance. A: Event-related changes of auto- and cross-spectra. The logarithm of the spectral value $S(t, f)$ was tested whether it was significantly different from the the spectral value $S(t_{ref}, f)$ in the reference segment ($t_{ref} = 2.0$–3.0 s). Red and yellow indicate a significant increase, white means insignificant values and blue indicates a significant decrease of PDC. B: Time-frequency map of event-related coherence changes. The coherences values are calculated by normalizing the cross-spectra with the corresponding autospectra. Again, a two-sample-test with $\alpha = 0.01$ was used for detecting statistically significant changes of the coherence values. The most significant coherence changes are observed in the alpha and beta frequencies between Fz-C3, C4-Fz, and C4-C3, although the cross-spectra for these channels do not show many statistical significant changes. C: Time-frequency map of the imaginary coherence (iCOH). While the coherence is also influenced by volume conduction, the iCOH represents only coupling with a time-delay. The iCOH is closely related to phase (see E:) A t-test was applied in order to test whether iCOH is zero or whether iCOH is significantly different from zero. D: Event-related changes of the imaginary coherence. A two-sample t-test was applied in order to test whether $iCOH(t,f)$ is significant different to $iCOH(t_{ref},f)$ in the reference interval $t_{ref} = 2.0$–3.0 s. E: Time-frequency maps of the phase differences between channels. A t-test was used to test whether the phase is significantly different than zero ($\alpha = 0.01$). Warm colors (yellow and red) indicate a phases significantly larger than zero, cold colors (green and blue) indicate negative phases. The time-frequency maps of the phases are very similar to the maps of the imaginary coherence (see Fig. 1-C). F: Time-frequency maps of the directed transfer function (DTF). Similar to PDC, the DTF provides another measure for the ''causality'' or information flow between channels. Here, DTF was tested with a simpe t-test ($\alpha = 0.01$) whether $DTF(t, f)$ is significantly larger than zero. G: Event-related partial directed coherence of left hand motor imagery. The PDC shows causal relationships between pairs of channel. Accordingly, leading and following channels can be distinguished, and the direction of the ''information flow'' can be obtained. By means of a two-sample t-test was tested whether the $PDC(t, f)$ at time t was significant different from $PDC(t_{ref}, f)$ at the reference interval $t_{ref} = 2.0$–3.0 s. Significant PDC changes are seen in beta and gamma range from C4 to all other channels, as well as in Fz->C4. H: Event-related partial directed coherence during right hand motor imagery. In this case, most interesting, PDC reveals a dominant coupling increase within the beta/gamma frequency range leading from Fz to C3. The homologue phenomenon can be observed during left hand motor imagery (Fig 1-G).

investigated, 5×5 T–F maps are shown for each channel pair.

(a) Event-related log S: The main diagonal (Fig. 1-A) contains all time-varying autospectra (or power-spectra) for each single recording position (channel), while the cross-spectra can be found off-diagonal. The event-related autospectra show which recording positions measured frequency-specific increases or decreases in relation to the baseline interval. A relative power decrease in the low frequency range ($\leqslant 7$ Hz) can be found at all five positions over most parts of the whole trial. The most prominent, event-related decreases in the alpha and beta range are found at position C3 and C4. The power decrease at C4 starts by second 3 in the alpha (frequency peak around 11 Hz) as well as in the beta frequency band (frequency peak around 27 Hz). The decrease of alpha power at C3 (around 11 Hz) begins around second 3, while the weaker decrease in the beta frequency appears slightly later around second 4. Some more significant decreases can be mentioned: at channels Fz and Cz a weaker beta decrease and at channel Pz a stronger but temporally very restricted alpha power decrease around second 3.

(b) Event-related COH: Most prominently, the coherence results (Fig. 1-B) indicate a broad-banded coupling increase within the alpha and beta frequency between C4–Fz, C4–C3, and C4–Cz. However, a short look on the cross-spectra (see Fig. 1-A) delivers a very different picture on this matter. Importantly, the cross-spectra of C4–Fz, C4–C3 do not change at all in alpha and beta frequency bands. Only the cross-spectrum of C4–Cz shows a significant attenuation in the beta frequency. Therefore, the significant changes between C4–Fz and C4–C3 can be explained by the decrease of alpha and beta power at C4 (see autospectrum of C4). Thus, in this case the coherence change between C4 and Cz is due to cross-spectral changes, whereas the coherence changes between C4–Fz and C4–C3 are just side effects of the massive power decrease at C4.

(c) Event-related iCOH: Evaluating the event-related results of the iCOH (Fig. 1-C), significant changes are present in the beta frequency between C4–C3, C4–Cz and, temporally more restricted, between C4–Cz starting around second 3.5. In all three pairs there are significant changes of iCOH toward more positive values (reddish colors) in respect to the baseline interval. From this event-related perspective, the changes on the three channel pairs look similar.

(d) iCOH: This figure provides the absolute values of the iCOH (Fig. 1-D) reached in the course of all time windows. For the channel pairs C4–C3 and C4–Cz, the event-related iCOH analysis revealed similar patterns in the beta frequency. However, by inspecting the absolute iCOH values it becomes apparent that the event-related change results from different magnitudes of iCOH present during the baseline interval. Since for C4–C3 the absolute magnitude of the phase shift is close to zero during the baseline interval, the phase shift increases during the movement imagery. For the channel pair C4–Cz, there is a high level of negative phase shifts during the baseline that vanishes during movement imagery (magnitude becomes smaller, getting close to zero). However, from the perspective of the event-related analysis both patterns result in a significant increase of the phase shifts between C4–C3 and C4–Cz.

(e) Phase S: The phase (Fig. 1-E) is symmetric in the sense that $\varphi_{ij}(f) = -\varphi_{ji}(f)$. As easily recognizable, the results of the phase are very similar to iCOH. In fact, the results of the statistical test are (almost) equal. Moreover, we can estimate the time delay from the phase; a phase of 0.25 rad (e.g., C3–Cz and C3–C4) at about 25 Hz corresponds to a time delay of 1.6 ms. This time delay analysis could be applied for the

whole T–F map, accordingly the time delay for each frequency component and each time segment can be obtained.

(f) Event-related DTF: The DTF (Fig. 1-F) reveals a different pattern of results compared to all findings presented before, because DTF differentiates between forward and backward coupling. In the present case, coupling patterns as revealed by DTF are similar to the patterns provided by PDC (Fig. 1-G). In addition to the PDC changes, a significant coupling increase from C3 to C4 around the 10 and 22 Hz can be observed. Given that DTF is sensitive not only to direct but also to indirect linkages, this divergent C3–C4 coupling pattern might be due to the representation of indirect couplings.

(g) Event-related PDC: The PDC provides a similar picture (see Fig. 1-G) than DTF (Fig. 1-F) because PDC can differ between forward and backward direction. The PDC level changes most prominently in channel pairs involving C4. Starting from C4, there is an evident decrease of PDC toward Fz and Cz around the 20–25 Hz frequencies. Increases of PDC are present above 30 Hz from C4 directed to C3, Cz, and Pz, while C4 receives stronger input from Fz.

As a matter of fact, the oscillatory connectivity patterns associated with channel C4 (close to the contralateral primary motor areas) seem to be particularly engaged during left-hand motor imagery. This is in agreement with the knowledge of contralateral recruitment of somatotopical sections of the primary motor cortex during actions and motor imagery (e.g., Jeannerod, 1994; Neuper and Pfurtscheller, 2001; Ehrsson et al., 2003; Michelon et al., 2006). Primary motor areas are under control of higher order motor areas located more frontally (such as portions of the premotor cortex, the cingulate motor zones, or the supplementary motor area). Interestingly, our PDC and DTF analyses revealed a dominant event-related increase of information transfer, directed from the frontal position Fz toward C4, within the beta/gamma frequency band. This pattern fits to the one we might expect, if feed forward coupling from the more frontally located higher motor areas (such as pre-SMA or premotor cortex) is transmitted to the contralateral primary motor area associated with the imagined hand movement. We have also analyzed the right-hand motor imagery task (Fig. 1-H), and we can find a hemispheric homologous pattern during right-hand movement imagery. That is, PDC and DTF reveal a respective coupling increase within the beta/gamma frequency range from Fz to C3. These results indicate the potential usefulness and the possible physiological meaning of EEG coupling measures. By means of the multivariate approach, the interacting activity between different brain areas can be investigated in more detail, with the high time-resolution of the EEG.

Practical issues

In order to apply MVAR methods, some parameters, such as model order, segment length, number of trials, and number of channels, have to be fixed a priori. In fact, the MVAR estimates can be degenerated if these parameters are set incorrectly. This problem can be avoided if some simple rules are taken into account.

(a) the model order p.
Various criteria have been proposed for the model order selection (Marple, 1987; Herrera et al., 1997). The difficulty of these criteria is that a wide variety of possible model orders are suggested, thus, no consistent model orders are obtained and in practice these criteria are not very helpful. Moreover, slight modification of the model hardly changes the spectra. Altogether, the importance of the model order selection seems to be often overestimated. As an alternative we recommend to use a fixed model order and to select the model order so that all points below are considered.
It is also known that the model order determines the number of modeled frequency components and in this sense it determines the "frequency resolution." As

a rule of thumb, the number of frequency components is half of the model order p. In case of multivariate analysis $M \cdot p/2$ frequency components (there are $M \cdot p$ roots of the characteristic polynomial $\det(A(z))$), these components are distributed among M channels. Therefore, $p/2$ frequency components are observed between each channel pair.

(b) Window length ΔT.
The longer the time window is, the more samples for estimating the MVAR are available. On the other hand, a longer time window means also a lower time resolution. A pragmatic solution is choosing the window length ΔT in such a way that it resembles roughly the expected time scale of interest. In this study, an imaginary hand movement task lasting for 4 s was used. Thus, we have chosen a time window of the length of 1 s (i.e., 250 samples).

(c) A general limitation of any T–F analysis is the principle of uncertainty between the time and frequency domain (Priestley, 1981). According to the uncertainty principle, the product of the time resolution ΔT and the frequency resolution ΔF is always $\Delta T \cdot \Delta F > c$ larger than some constant c. For the single trial case is $c = 1$, in case of ensemble averaging of m trials is $c = 1/\sqrt{(m)}$. It is reasonable to assume that the frequency resolution is approximated by $\Delta F = F_s/p$, the sampling rate divided by the model order. Hence the following equation should be fulfilled: $\Delta T \cdot F_s \sqrt{(m) > p}$. A violation of this requirement will cause large estimation errors in the T–F results, hardly any statistically significant result can be obtained.

(d) Estimation theory shows that the number of samples should be larger than the number of estimates. In case of MVAR estimation, we have $M^2 \cdot p$ estimates and $M \cdot N \cdot m$ sample values ($N = \Delta T \cdot F_s$ is the number of samples per trial), hence the ratio $(M \cdot N \cdot m)|(M^2 \cdot p) = (N \cdot m)/(M \cdot p)$ must be larger than 1 (Kus et al., 2004). As a rule of thumb, a ratio of 10 or larger is recommended. If this rule is not fulfilled, the error in the MVAR estimates will become large.

If someone needs to select the above parameters, one should take care that each point is fulfilled. If any of these recommendations are violated, it is likely that the MVAR analysis will fail (e.g., in the case that the number of samples is to small, no robust estimates can be obtained). Ideally, these parameters should be already fixed in the course of the experimental design.

In this study, $M = 5$ channels, a model order of $p = 15$, a window length of $\Delta T = 1$ s, a sampling rate $F_s = 250$ Hz, and $m = 90–1 = 89$ trials (because of LOOM) were used. Accordingly, up to 32 frequencies might be resolved, for each channel pair up to seven frequency components in the range of 0–125 Hz are available. The recommendation derived from the uncertainty principle $\Delta T \cdot F_s \sqrt{(m)} = 250 \cdot \sqrt{90} = 2372 > p = 15$ is fulfilled. This is also true for the ratio between the number of sample values and the number of estimates, $(N \cdot m)/(M \cdot p) = 250 \cdot 90/(5 \cdot 15) = 300 \gg 1$, which is much larger than 1. Hence, in this work the recommendations mentioned above are fulfilled.

Summary

This study describes the use of MVAR parameters and their derived coupling measures in the context of event-related EEG analysis. We addressed the issue of statistical significance tests and, specifically, we considered the application of resampling methods used for estimating confidence intervals. To obtain group statistics it is computationally even less demanding, since this case makes resampling superfluous. The confidence interval can be simply obtained from the standard error of the group.

A general problem associated with classical coherence is that it is incapable of distinguishing between true cortical interactions and volume conduction (Florian et al., 1998; Andrew and Pfurtscheller, 1999; Pfurtscheller and Andrew, 1996). The phase is often thought to be independ-

ent of volume conduction. Nevertheless, a large volume conduction effect can cause a bias towards zero phase. The pCOH removes volume conduction effects, but does not provide a direction of information transfer. Only PDC (Baccala and Sameshima, 2001), DTF (Kaminski et al., 2001; Korzeniewska et al., 2003), and iCOH (Nolte et al., 2004) provide the direction of information transfer and are not influenced by the volume conduction effect. Therefore, PDC, DTF, and iCOH are the most interesting measures for describing couplings between EEG signals.

It is noteworthy that PDC and DTF (including PDCF, ffDTF, and dDTF) describe a property that is qualitatively different from phase or coherency (including classical coherence, phase, and time delay). Even though the phase information and the iCOH provide directional information, the phase between channels i and j has the same magnitude than in the reverse direction (from channel j to i), only the sign changes. The same is true for the iCOH. In contrary, PDC and DTF are not symmetric at all: the forward connection can yield a large value (e.g., close to 1), whereas the backward connection can be almost zero. Thus, PDC and DTF describe different properties from coherency and can hardly be compared to phase or iCOH.

Baccala and Sameshima (2001) claimed that PDC is superior to DTF because it provides large values only for the case of a "direct connection." This claim implicitly assumes that all "sources" are recorded (provided that the sources originate from the cortex and can be detected by EEG electrodes). Mathematically, the differences between DTF and PDC correspond to different terms of normalization: since PDC is calculated with respect to all outflows, DTF is normalized by all inflows (see Kus et al., 2004). PDC and DTF are attractive measures, since they are capable of describing couplings in forward and backward direction in the context of causality analysis. However, one must be aware that an analysis on causality is only reasonable if the activity of all sources is recorded. Kus et al. (2005, p. 221) reported that "pairwise estimates — bivariate Granger causality … may give totally confusing results". This warning is equally valid for any other case, where sources are not directly available (sources not covered by EEG electrodes or sources originating from some lower brain areas, e.g., thalamic sources). Hence, the importance of this limitation has still to be assessed. In the case that all major sources reside in the cortex and are captured by EEG channels, this limitation becomes invalid and so we gain the advantage of assessing the information flow between positions in forward and backward direction through PDC.

In conclusion, the MVAR-based methods provide a powerful set of tools for investigating the various aspects of multichannel spectral properties of EEG. From a general point of view, the MVAR approach can be seen to bridge two different areas of signal processing. On the one side, classical phase analysis as obtained equally by methods of deterministic signal processing, on the other side, methods that use the field of causal analysis in the context of stochastic time series analysis (TSA).

References

Andrew, C. and Pfurtscheller, G. (1999) Lack of bilateral coherence of post-movement central beta oscillations in the human electroencephalogram. Neurosci. Lett., 273: 89–92.

Babiloni, F., Cincotti, F., Babiloni, C., Carducci, F., Mattia, D., Astolfi, L., Basilisco, A., Rossini, P.M., Ding, L., Ni, Y., Cheng, J., Christine, K., Sweeney, J. and He, B. (2005) Estimation of the cortical functional connectivity with the multimodal integration of high-resolution EEG and fMRI data by DTF. Neuroimage, 24: 118–131.

Baccala, L.A. and Sameshima, K. (2001) Partial directed coherence: a new concept in neural structure determination. Biol. Cybern., 84: 463–474.

Blinowska, K.J., Kus, R. and Kaminski, M. (2004) Granger causality and information flow in multivariate processes. Phys. Rev. E. Stat. Nonlin. Soft Matter Phys., 70: 050902.

Efron, B. (1981) Nonparametric estimates of standard error: the jackknife, the bootstrap and other methods. Biometrika, 68: 589–599.

Ehrsson, H.H., Geyer, S. and Naito, E. (2003) Imagery of voluntary movement of fingers, toes, and tongue activates corresponding body-part-specific motor representations. J. Neurophysiol., 90: 3304–3316.

Fenwick, P.B., Mitchie, P., Dollimore, J. and Fenton, G.W. (1969) Application of the autoregressive model to EEG analysis. Agressologie, 10: 553–564.

Fenwick, P.B., Mitchie, P., Dollimore, J. and Fenton, G.W. (1970a) The use of the autoregressive model in EEG analysis. Electroencephalogr. Clin. Neurophysiol., 29: 327.

Fenwick, P.B., Mitchie, P., Dollimore, J. and Fenton, G.W. (1970b) The use of the autoregressive model in EEG analysis. Electroencephalogr. Clin. Neurophysiol., 29(3): 327.

Fenwick, P.B., Mitchie, P., Dollimore, J. and Fenton, G.W. (1971) Mathematical simulation of the electroencephalogram using an autoregressive series. Int. J. Biomed. Comput., 2: 281–307.

Fiebach, C.J., Gruber, T. and Supp, G.G. (2005) Neuronal mechanisms of repetition priming in occipitotemporal cortex: spatiotemporal evidence from functional magnetic resonance imaging and electroencephalography. J. Neurosci., 25: 3414–3422.

Florian, G., Andrew, C. and Pfurtscheller, G. (1998) Do changes in coherence always reflect changes in functional coupling? Electroencephalogr. Clin. Neurophysiol., 106: 87–91.

Fries, P. (2005) A mechanism for cognitive dynamics: neuronal communication through neuronal coherence. Trends Cogn. Sci., 9: 474–480.

Gardner, W.A. (1992) A unifying view of coherence in signal processing. Signal Process., 29: 113–140.

Gersch, W. (1970) Spectral analysis of EEG's by autoregressive decomposition of time series. Math. Biosci., 7: 205–222.

Granger, C.W.S. (1969) Investigating causal relations by econometric methods and cross-spectral methods. Econometrica, 37: 424–438.

Gruber, T., Muller, M.M. and Keil, A. (2002) Modulation of induced gamma band responses in a perceptual learning task in the human EEG. J. Cogn. Neurosci., 14: 732–744.

Herrera, R.E., Sun, M., Dahl, R.E., Ryan, N.D. and Sclabassi, J., (1997) Vector autoregressive model selection in multichannel EEG, 19th International Conference IEEE/EMBS, Chicago.

Jeannerod, M. (1994) The representing brain: neural correlates of motor intention and imagery. Behav. Brain Sci., 17: 187–245.

Kaminski, M.J. and Blinowska, K.J. (1991) A new method of the description of the information flow in the brain structures. Biol. Cybern., 65: 203–210.

Kaminski, M., Blinowska, K. and Szelenberger, W. (1995) Investigation of coherence structure and EEG activity propagation during sleep. Acta. Neurobiol. Exp. (Wars.), 55: 213–219.

Kaminski, M., Blinowska, K. and Szclenberger, W. (1997) Topographic analysis of coherence and propagation of EEG activity during sleep and wakefulness. Electroencephalogr. Clin. Neurophysiol., 102: 216–227.

Kaminski, M., Ding, M., Truccolo, W.A. and Bressler, S.L. (2001) Evaluating causal relations in neural systems: granger causality, directed transfer function and statistical assessment of significance. Biol. Cybern., 85: 145–157.

Korzeniewska, A., Manczak, M., Kaminski, M., Blinowska, K.J. and Kasicki, S. (2003) Determination of information flow direction among brain structures by a modified directed transfer function (dDTF) method. J. Neurosci. Methods, 125: 195–207.

Kus, R., Blinowska, K.J., Kaminski, M. and Basinska-Starzycka, A. (2005) Propagation of EEG activity during continuous attention test. Bull. Polish Acad. Sci., 53(3): 217–222.

Kus, R., Kaminski, M. and Blinowska, K.J. (2004) Determination of EEG activity propagation: pair-wise versus multichannel estimate. IEEE Trans. Biomed. Eng., 51: 1501–1510.

Lustick, L.S., Saltzberg, B., Buckley, J.K. and Heath, R.G. (1968) Autoregressive model for simplified computer generation of EEG correlation functions, Annual Conference on Engineering in Medicine and Biology. IEEE, New York, NY, USA.

Marple, S.L. (1987) Digital Spectral Analysis with Applications. Prentice Hall, Englewood Cliffs, NJ.

Michelon, P., Vettel, J.M. and Zacks, J.M. (2006) Lateral somatotopic organization during imagined and prepared movements. J. Neurophysiol., 95: 811–822.

Neuper, C. and Pfurtscheller, G. (2001) Evidence of distinct beta resonance frequencies in human EEG related to specific sensorimotor cortical areas. Clin. Neurophysiol., 112: 2084–2097.

Nolte, G., Bai, O., Wheaton, L., Mari, Z., Vorbach, S. and Hallett, M. (2004) Identifying true brain interaction from EEG data using the imaginary part of coherency. Clin. Neurophysiol., 115: 2292–2307.

Nunez, P.L., Silberstein, R.B., Shi, Z., Carpenter, M.R., Srinivasan, R., Tucker, D.M., Doran, S.M., Cadusch, P.J. and Wijesinghe, R.S. (1999) EEG coherency II: experimental comparisons of multiple measures. Clin. Neurophysiol., 110: 469–486.

Nunez, P.L., Srinivasan, R., Westdorp, A.F., Wijesinghe, R.S., Tucker, D.M., Silberstein, R.B. and Cadusch, P.J. (1997) EEG coherency. I: Statistics, reference electrode, volume conduction, Laplacians, cortical imaging, and interpretation at multiple scales. Electroencephalogr. Clin. Neurophysiol., 103: 499–515.

Pfurtscheller, G. and Andrew, C. (1999) Event-related changes of band power and coherence: methodology and interpretation. J. Clin. Neurophysiol., 16: 512–519.

Pfurtscheller, G. and Aranibar, A. (1977) Event-related cortical desynchronization detected by power measurements of scalp EEG. Electroencephalogr. Clin. Neurophysiol., 42: 817–826.

Pfurtscheller, G., Brunner, C., Schlögl, A. and Lopes da Silva, F.H. (2006) Mu-rhythm (de)synchronization and EEG single-trial classification of different motor imagery tasks. Neuroimage, 31(1): 153–159.

Pfurtscheller, G. and Haring, G. (1972) The use of an EEG autoregressive model for the time-saving calculation of spectral power density distributions with a digital computer. Electroencephalogr. Clin. Neurophysiol., 33: 113–115.

Pfurtscheller, G. and Lopes da Silva, F.H. (1999) Event-related EEG/MEG synchronization and desynchronization: basic principles. Clin. Neurophysiol., 110: 1842–1857.

Priestley, M.B. (1981) Spectral Analysis and Time Series. Academic Press, London, UK.

Sameshima, K. and Baccala, L.A. (1999) Using partial directed coherence to describe neuronal ensemble interactions. J. Neurosci. Methods, 94: 93–103.

Schlögl, A. (2006) A comparison of multivariate autoregressive estimators. Signal Process, 86(9): 2426–2429.

Schlögl, A., Lee, F.Y., Bischof, H. and Pfurtscheller, G. (2005) Characterization of four-class motor imagery EEG data for the BCI-competition 2005. J. Neural Eng., 2: 14–22.

Schneider, T. and Neumaier, A. (2001) Algorithm 808: ARfit – A Matlab package for the estimation of parameters and eigenmodes of multivariate autoregressive models. ACM Trans. Math. Softw., 27: 58–65.

Supp, G.G., Schlögl, A., Fiebach, C.J., Gunter, T.C., Vigliocco, G., Pfurtscheller, G. and Petsche, H. (2005) Semantic memory retrieval: cortical couplings in object recognition in the N400 window. Eur. J. Neurosci., 21: 1139–1143.

Supp, G.G., Schlögl, A., Gunter, T.C., Bernard, M., Pfurtscheller, G. and Petsche, H. (2004) Lexical memory search during N400: cortical couplings in auditory comprehension. Neuroreport, 15: 1209–1213.

Varela, F., Lachaux, J.P., Rodriguez, E. and Martinerie, J. (2001) The brainweb: phase synchronization and large-scale integration. Nat. Rev. Neurosci., 2: 229–239.

Wiggins, R.A. and Robinson, E.A. (1965) Recursive solution to the multichannel filtering problem. J. Geophys. Res., 70: 1885–1891.

Wright, J.J. and Lily, D.T.J. (1996) Dynamics of the brain at the global and microscopic scales – neural networks and the EEG. Behav. Brain Sci., 19: 285–293.

Zetterberg, L.H. (1969) Estimation of parameter for linear difference equation with application to EEG analysis. Math, Biosci., 5: 227–275.